Adaptive Motion Planning via Dynamic Constraint Satisfaction (Appendix)

Constraint Satisfaction Modeling

We formulate the functions to evaluate the constraint satisfaction degree in the paper. To evaluate the satisfaction of relaxable constraints, we set up three membership functions according to the relationship between the $\mathcal{X}_{i,k}$ and the target values. The three functions are $\mathrm{DS}^1(\mathcal{X}_{i,k})$, $\mathrm{DS}^2(\mathcal{X}_{i,k})$, and $\mathrm{DS}^3(\mathcal{X}_{i,k})$ based on the relationship of LESS THAN, MORE THAN and AS CLOSE AS POSSIBLE. $\mathrm{DS}^0(\mathcal{X}_{i,k})$ is the function to evaluate the satisfaction of unrelaxable constraints. Correspondingly, the functions to evaluate constraint satisfaction are listed as follows:

$$\mathrm{DS}^1(\mathcal{X}_{i,k}) = \begin{cases} 1 & \mathcal{X}_{i,k} \le g_i \\ \frac{ub_i - \mathcal{X}_{i,k}}{ub_i - g_i} & g_i < \mathcal{X}_{i,k} \le ub_i \\ 0 & otherwise \end{cases}$$

$$\mathrm{DS}^2(\mathcal{X}_{i,k}) = \begin{cases} \frac{\mathcal{X}_{i,k} - lb_i}{g_i - lb_i} & lb_i \le \mathcal{X}_{i,k} < g_i \\ 1 & \mathcal{X}_{i,k} \ge g_i \\ 0 & otherwise \end{cases}$$

$$\mathrm{DS}^3(\mathcal{X}_{i,k}) = \begin{cases} \frac{\mathcal{X}_{i,k} - lb_i}{g_i - \sigma_i - lb_i} & lb_i \le \mathcal{X}_{i,k} < g_i - \sigma_i \\ 1 & g_i - \sigma_i \le \mathcal{X}_{i,k} \le g_i + \sigma_i \\ \frac{ub_i - \mathcal{X}_{i,k}}{ub_i - g_i - \sigma_i} & g_i + \sigma_i < \mathcal{X}_{i,k} \le ub_i \\ 0 & otherwise \end{cases}$$

$$\mathrm{DS}^0(\mathcal{X}_{i,k}) = \begin{cases} 1, & \text{if } \mathcal{X}_{i,k} \text{ satisfies } C_i \in \mathcal{C}_{nr} \\ 0, & \text{otherwise} \end{cases}$$

- Safety: Supposing that the set of obstacles detected by the AMR at time instant k is $\mathcal{O}_k$, while the current state of AMR is $\boldsymbol{s}_k$. The distance between AMR and the center of obstacle reflects the safety risk. Thus, the indicator of safety constraint is $\mathcal{X}_{S_{o,k}} = \frac{\|\boldsymbol{x}_k - \boldsymbol{x}_o\|_2 - r_a - r_o}{D_o}, \forall o \in \mathcal{O}_k$. The constraint satisfaction function is as below:

$$\mathrm{DS}^2(\mathcal{X}_{S_{o,k}}) = \begin{cases} 0, & \mathcal{X}_{S_{o,k}} < 0 \\ 1, & \mathcal{X}_{S_{o,k}} \ge 1 \\ \mathcal{X}_{S_{o,k}}, & otherwise \end{cases}$$

  The normalized slack variable for the time instant k is $\overline{\zeta_{S,k}} = \sum_{o \in \mathcal{O}_k} \frac{\zeta_{S_{o,k}}}{|\mathcal{O}_k|}$.

- Privacy: Since the privacy risk depends on the distance between the AMR and the private region, as well as the working states of sensors (Luo et al. 2020), the indicator of privacy constraint at time instant k is defined as $\mathcal{X}_{P_{p,k}} = 1 - \|\boldsymbol{w}_k\| \frac{(r_a + r_p + D_p) - \|\boldsymbol{x}_k - \boldsymbol{x}_p\|_2}{D_p}, \forall p \in \mathcal{P}_k$. The constraint satisfaction function is as below:

$$\mathrm{DS}^2(\mathcal{X}_{P_{p,k}}) = \begin{cases} 0, & \|\boldsymbol{x}_k - \boldsymbol{x}_p\|_2 < r_a + r_p, \\ 1, & \mathcal{X}_{P_{p,k}} \ge 1, \\ \mathcal{X}_{P_{p,k}}, & otherwise \end{cases} \quad (1)$$

  The normalized slack variable for the time instant k is $\overline{\zeta_{P,k}} = \sum_{p \in \mathcal{P}_k} \frac{\zeta_{P_{p,k}}}{|\mathcal{P}_k|}$.

- Timelines: The indicator of timeliness is the motion time $\mathcal{X}_\xi = T\tau$, the constraint satisfaction function is as below:

$$\mathrm{DS}^1(\mathcal{X}_\xi) = \begin{cases} 1, & \mathcal{X}_\xi \le \Delta_t \\ \dfrac{\Delta - \mathcal{X}_\xi}{\Delta - \Delta_t}, & \Delta_t < \mathcal{X}_\xi \le \Delta \\ 0, & \mathcal{X}_\xi > \Delta \end{cases}$$

  The normalized slack variable is $\overline{\delta_{\xi,T}} = \frac{\delta_{\xi,T}}{\Delta - \Delta_t}$.

- Energy-saving: The energy consumption can be affected by the traveled distance, control effort, and sensor usage (Xiong and Shan 2018). At the time duration $[k\tau, (k+1)\tau)$, the energy cost is computed as $E_k = \|\boldsymbol{x}_{k+1} - \boldsymbol{x}_k\|_2 + \eta_1 \|\boldsymbol{v}_{k+1} - \boldsymbol{v}_k\|_2 + \eta_2 \|\boldsymbol{\omega}_k\| \tau$ with the assumption that each unit of traveled distance costs one unit of energy, deceleration or acceleration costs η_1 units, and sensor usage costs η_2 units of energy. The indicator of energy consumption is $\mathcal{X}_E = \sum_{k=0}^{T-1} E_k$; the constraint satisfaction function is as below:

$$\mathrm{DS}^1(\mathcal{X}_E) = \begin{cases} 1, & \mathcal{X}_E \le E_t \\ \dfrac{E - \mathcal{X}_e}{E - E_t}, & E_t < \mathcal{X}_e \le E \\ 0, & \mathcal{X}_E > E \end{cases}$$

  The normalized slack variable is $\overline{\delta_{E,T}} = \frac{\delta_{E,T}}{E - E_t}$.

- Accuracy: The average quality of the information collected during the mission is denoted as $\mathcal{X}_\varphi = \frac{1}{T\tau} \sum_{k=0}^{T-1} \|\boldsymbol{w}_k\| \tau$; the constraint satisfaction function is

as below:

$$\mathrm{DS}^2(\mathcal{X}_\varphi) = \begin{cases} 0, & \mathcal{X}_\varphi < A \\ \dfrac{\mathcal{X}_\varphi - A}{A_t - A}, & A \le \mathcal{X}_\varphi < A_t \\ 1, & \mathcal{X}_\varphi \ge A_t \end{cases}$$

The normalized slack variable is $\overline{\zeta_{\varphi,T}} = \frac{\zeta_{\varphi,T}}{A_t - A}$.

Quadrotor Experimental Results

We show the details of the experimental results with the quadrotor discussed in the paper.

Scalability To demonstrate the scalability of ACMP for different scales of environments, we further simulate the quadrotor in two selected real urban environments extracted from the open building dataset of Portland in USA (Burian et al. 2002). We used ArcGIS map to set up a 3D model based on the method in (Hidalgo-Panagua et al. 2017). The original space of these two environments is $500 \times 500 \times 100m^3$ and $10^3 \times 10^3 \times 100\ m^3$, respectively. And the space is then compressed into $50 \times 50 \times 10$ and $100 \times 100 \times 10$, respectively. The dataset provides the central location (longitude and latitude), average height, and building types (i.e., industrial and commercial buildings, houses, and apartments to live in) of each building. The buildings for industrial and commercial use are viewed as obstacles, while houses and apartments are viewed as private regions. As shown in Fig. 2, the process of real urban scenario modeling is explained. We set the range of longitude and latitude of working space on the ArcGIS map, and all the buildings are marked as blue (Fig. 2(a)). Then the ArcGIS map is turned into a binary map. Thus a 3D model of the urban scenario is set up with the scale of $500m \times 500m \times 100m$ in Fig. 2(c). So as to scenario construction for the scale of $1000m \times 1000m \times 100m$ in Fig. 3.

In each case, the flight task of the quadrotor is to travel from the position $[0, 0, 0]$ to the destination $[49, 49, 0]$ and $[99, 99, 0]$ respectively. During the flight, the quadrotor is expected to follow constraints of safety, privacy, timeliness, accuracy, and energy-saving. The flight path, velocity, sensor configurations and constraint achievement of the quadrotor at each time instant are shown in Fig. 2(d), Fig. 2(e) and Fig. 2(f). The flight trajectory of the quadrotor with ACMP in the scale of $1000m \times 1000m \times 100m$ is shown in Fig. 3.

Table 1 summarizes the experimental results in these two scales of environment. As shown in the Table 1, in the scale of $1000m \times 1000m \times 100m$, the flight task is completed at 60.07 s, consuming 106.27 units of energy without safety and privacy risk. In the scale of $1000m \times 1000m \times 100m$, the task is finished at 101.5 s, consuming 210.94 units of energy. The generated trajectory does not have safety risk but 4 points along the trajectory violate relaxable privacy constraint, resulting in an average 99.98% satisfaction of the privacy constraint. In contrast, SCMP fails to find feasible motion plans at runtime when the scale of working space increases.

Choice of violation tolerance Given a set of violation tolerances, the possibilities that relaxable constraints

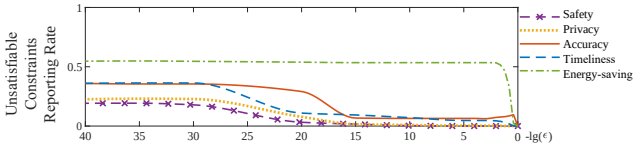

Figure 1: Unsatisfiable constraints reporting rate. (Quadrotor case, $\rho_o = 2\%, \rho_p = 2\%$)

are reported as unsatisfiable are recorded per simulation, as shown in Fig. 1. We choose $\varepsilon_{S,P,\xi,E,\varphi} = \{10^{-20}, 10^{-20}, 10^{-20}, 0.005, 10^{-10}\}$ in the quadrotor simulation. Thanks to the setting of violation tolerance, 16.0%, 14.7%, 29.0%, 25.5%, and 1.1% of relaxable constraint violations are not reported for constraints of safety, privacy, timeliness, accuracy, and energy-saving, respectively. This filter fewer number of constraints into $\mathcal{C}_{na}$, improving robot real-time performance as the *Constraints Satisfaction Optimization* step is less triggered. These results show that choosing the right violation tolerance parameters can help determine the appropriate set of unsatisfied constraints with a smaller impact on the algorithm's efficiency. In the case that the choice of tolerance parameter may affect the convergence in the *constraints Satisfaction Optimization* step and result in no feasible solutions, ACMP can directly leverage the planning results from the *constraints Satisfaction Checking* step, as illustrated in Algorithm 1.

UUV Oceanic Surveillance

This example originates from (Shevtsov and Weyns 2016; Shevtsov, Weyns, and Maggio 2019). Rather than considering single-objective optimization for the UUV scenario in (Shevtsov and Weyns 2016), we extended it to achieve multiple constraints under uncertainties and disturbances, while other parameters like sensor configurations are kept the same, as shown in Table 2. The constraints to meet in this scenario are listed as follows:

- Scanning Distance (C_l): A segment of the surface over a distance of $L_t = 100$ km is expected to be examined by the UUV within $\Delta = 10$ hours, while the unrelaxable constraint of surveillance distance is $L = 90$ km.
- Energy Consumption (C_E): A total amount of energy $E_t = 5.4$ MJ is expected to be consumed, while the maximum amount of energy is $E = 6$ MJ.
- Accuracy (C_φ): The accuracy of measurements is targeted at $A_t = 90\%$, while the unrelaxable accuracy constraint is set as $A = 80\%$.

Constraints Satisfaction Modeling

The UUV is equipped with 5 onboard sensors for ocean surveillance. The scanning time 10 hours is divided into 360 time instance. $x_i, i \in [1, 5]$ is the portion of time the sensor i should be used during system operation in each instance. Acc_i is the accuracy of sensor i; E_i is the energy consumed by sensor; V_i is the scanning speed of sensor. q_i is the portion of sensor accuracy and p_i is the portion of scanning speed,

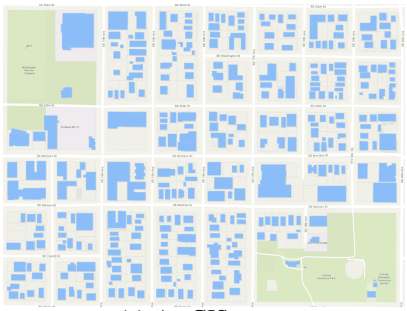

(a) ArcGIS map.

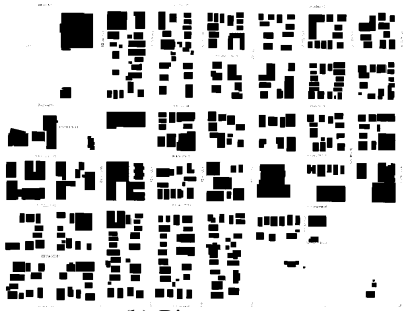

(b) Binary map.

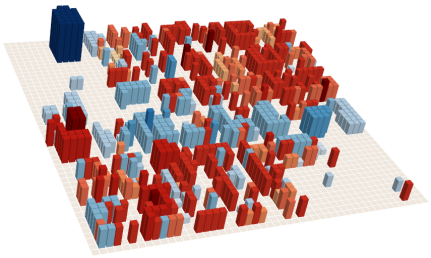

(c) Grid map.

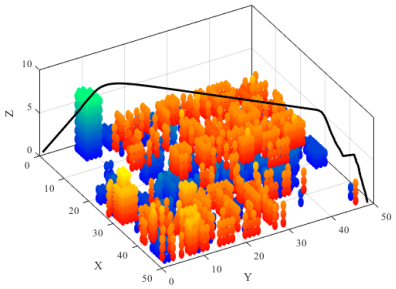

(d) Flight path of the quadrotor.

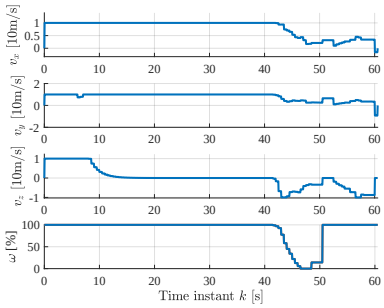

(e) Velocity and sensor configurations.

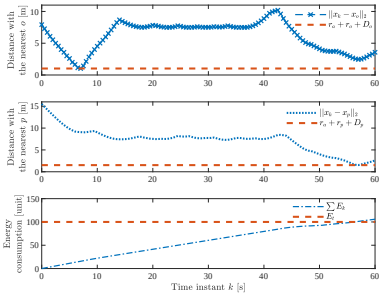

(f) Constraint satisfaction during the flight.

Figure 2: Environment Modeling and Flight Trajectory of the Quadrotor with ACMP. ($500m \times 500m \times 100m$).

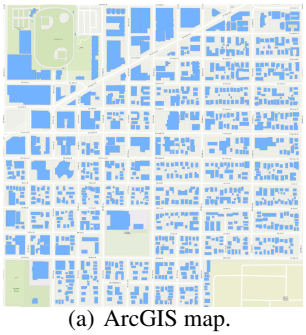

(a) ArcGIS map.

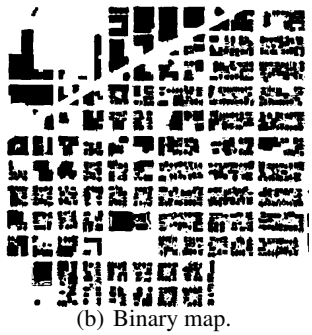

(b) Binary map.

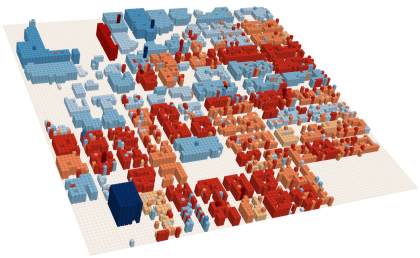

(c) Grid map.

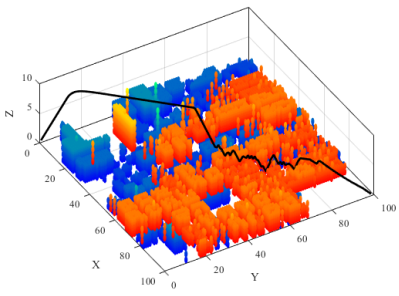

(d) Flight path of the quadrotor.

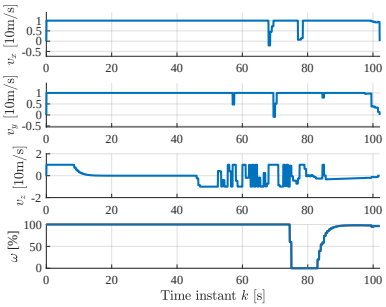

(e) Velocity and sensor configurations.

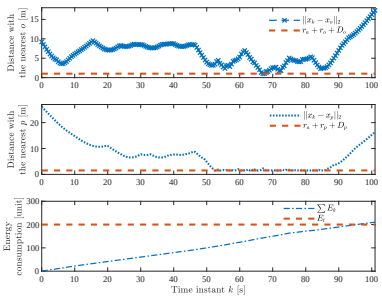

(f) Constraint satisfaction during the flight.

Figure 3: Environment Modeling and Flight Trajectory of the Quadrotor with ACMP. ($1000m \times 1000m \times 100m$)

Table 1: Adaptive-Constrained Motion Planning Results for Different Scales of Environments

Scale		*Accuracy* [%]	*Traveling Time* [s]	*Energy Consumption* [unit]	*Safety*	*Privacy*	*Real-time Performance*
50	$\mathcal{C}_r$	A_t=90	Δ_t=60	E_t=100	D_o=5m	D_p=10m	Adaptation Rate
	$\mathcal{C}_{nr}$	A=80	Δ=90	E=150	r_o=5m	r_p=5m	6/120
	$\mathcal{X}$	90	60.00	105.57	0	0	Overhead
	$\mathcal{DS}$	100%	100%	88.85%	100%	100%	Avg. 0.066s Std. 0.139s
100	$\mathcal{C}_r$	A_t=90	Δ_t=90	E_t=200	D_o=5m	D_p=10m	Adaptation Rate
	$\mathcal{C}_{nr}$	A=80	Δ=150	E=300	r_o=5m	r_p=5m	3/203
	$\mathcal{X}$	90	101.50	210.94	0	0.1534	Overhead
	$\mathcal{DS}$	100%	80.83%	89.06%	100%	99.98%	Avg. 0.132s Std. 0.180s

Table 2: Parameters of sensors of the UUV.

UUV onboard sensor	Energy cons. J/s	Scan Speed m/s	Accuracy %
1	170	2.6	97
2	135	3.6	89
3	118	2.6	83
4	100	3.0	74
5	78	3.6	49

respectively in decimals. The energy consumption is related with accuracy and scanning speed of the sensor. The corresponding indicators for the three constraints are formulated as: $\mathcal{X}_l = \sum_{k=0}^{T}\sum_{i=0}^{N} x_i q_i V_i \tau$, $\mathcal{X}_E = \sum_{k=0}^{T}\sum_{i=0}^{N} x_i E_i \cdot \frac{e^{p_i+q_i}-1}{e^2-1}\tau$, and $\mathcal{X}_\varphi = \sum_{k=0}^{T}\sum_{i=0}^{N} x_i p_i Acc_i$, where $T = 360$, i.e., the time step τ is 100s and the time instance k incremented by $1 \sim 360$. The constraint satisfaction functions are shown as follows:

- Scanning distance (C_l):

$$\mathrm{DS}^2(\mathcal{X}_l) = \begin{cases} 0, & \mathcal{X}_l < L \\ \dfrac{\mathcal{X}_l - L}{L_t - L}, & L \le \mathcal{X}_l < L_t \\ 1, & \mathcal{X}_l \ge L_t \end{cases}$$

  The normalized slack variable is $\overline{\zeta_{l,T}} = \frac{\zeta_{l,T}}{L_t - L}$.

- Energy consumption (C_E):

$$\mathrm{DS}^1(\mathcal{X}_E) = \begin{cases} 1, & \mathcal{X}_E \le E_t \\ \dfrac{E - \mathcal{X}_E}{E - E_t}, & E_t < \mathcal{X}_E \le E \\ 0, & \mathcal{X}_E > E \end{cases}$$

  The normalized slack variable is $\overline{\delta_{E,T}} = \frac{\delta_{E,T}}{E - E_t}$.

- Accuracy (C_φ):

$$\mathrm{DS}^2(\mathcal{X}_\varphi) = \begin{cases} 0, & \mathcal{X}_\varphi < A \\ \dfrac{\mathcal{X}_\varphi - A}{A_t - A}, & A \le \mathcal{X}_{\varphi_k} < A_t \\ 1, & \mathcal{X}_\varphi \ge A_t \end{cases}$$

  The normalized slack variable is $\overline{\zeta_{\varphi,T}} = \frac{\zeta_{\varphi,T}}{A_t - A}$.

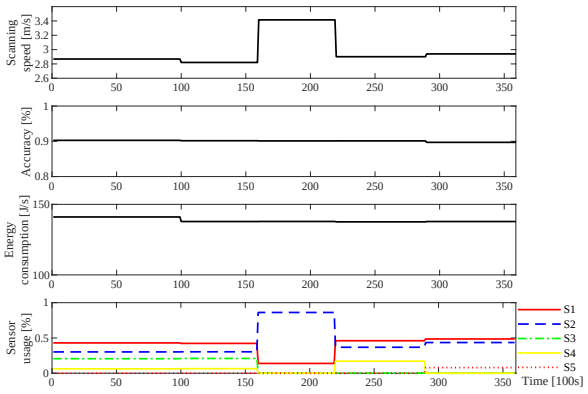

Figure 4: Adaptive-Constrained Motion Planning Results in the UUV Case.

Experimental Results

To demonstrate the generality of ACMP, we applied it to a UUV case described in (Shevtsov and Weyns 2016). The constraint satisfaction functions in this scenario are $\mathrm{DS}^1(\mathcal{X}_l)$ (scanning distance), $\mathrm{DS}^2(\mathcal{X}_E)$ (energy consumption) and $\mathrm{DS}^2(\mathcal{X}_\varphi)$ (accuracy). There are trade-offs between the satisfaction of these constraints, e.g., when sensors (e.g., sensor 1) with a higher quality of surveillance is chosen, more energy is consumed, resulting in less distance scanned.

Effectiveness The Fig. 4 shows the adaptive-constrained motion planning results of the UUV during operation with the case in (Shevtsov and Weyns 2016). At time instant $k = 100$, we change the target energy consumption (E_t) from 5.4 MJ to 5.0 MJ; at $k = 160$, we change the distance expected to be scanned (L_t) from 100 km to 105 km. Fig. 4 shows that changes in the target values of constraints lead to rearrangement of the sensor usage, as the time portion for $S2$ increases. Fig. 4 also shows how ACMP reacts to changes in sensor parameters and sensor failures. At $k = 220$, the measurement accuracy of sensor $S3$ drastically decreases from 83% to 43%, and $S4$ stops working at $k = 290$, this leads to a suboptimal solution that $S1$ is more exploited. Finally, the mission ends with average measurement accuracy of 90.1%,

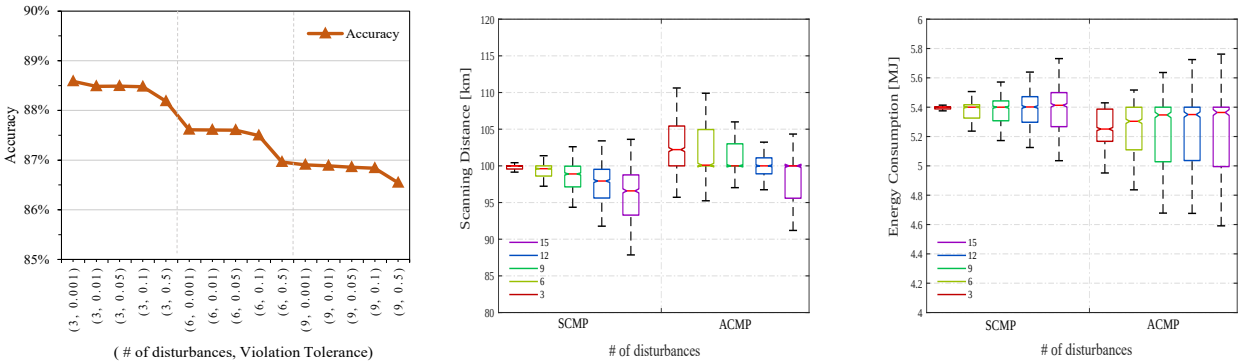

(a) Scanning accuracy with various disturbances and ε. (ACMP)

(b) Variance of scanning distance.

(c) Variance of energy consumption.

Figure 5: Scanning accuracy, distance and energy consumption with various probability of disturbances and violation tolerance.

Table 3: Constraints Satisfaction Results in the UUV Case.

Indicators	*Approaches*	# of disturbances				
		3	6	9	12	15
$\mathcal{X}_\varphi$ [%]	SCMP	88.9	87.5	85.8	84.4	82.4
	ACMP	***89.6***	***88.4***	***87.0***	***85.4***	***83.2***
$\mathcal{X}_l$ [km]	SCMP	99.9	99.2	98.0	96.6	94.5
	ACMP	***104.2***	***104.0***	***103.5***	***101.0***	***98.9***
$\mathcal{X}_E$ [MJ]	SCMP	5.34	5.33	5.31	5.34	5.34
	ACMP	***5.24***	***5.18***	***5.14***	***5.16***	***5.16***

[a] The violation tolerance are $\varepsilon_l = 0$, $\varepsilon_E = 0$, and $\varepsilon_\varphi = 10^{-3}$.

scanning distance of 106.7 km, and energy consumption of 4.98 MJ.

Robustness In this case, the robustness of ACMP and SCMP is compared while adding disturbances to sensors' parameters (i.e., sensor accuracy, scanning speed, and energy consumption) at random time instants. For each frequency of disturbances, we simulated 500 rounds and computed the average accuracy, scanning distance, and energy consumption. The results are shown in Table 3. We can see that under ACMP, the UUV can scan a longer distance with higher accuracy and less energy consumption than SCMP. Moreover, the motion generated by SCMP can hardly satisfy all the three constraints, while the motion generated by ACMP can satisfy the timeliness and energy constraints, only slightly violating the accuracy constraint. The reason behind this is that at the *Constraints Satisfaction Analysis* stage, the accuracy constraint is mostly selected as the objective function to optimize while the other two constraints are remained as their initial formulas. The variance of scanning distance and energy consumption of two approaches are compared in Fig. 5(b) and Fig. 5(c).

Real-time Performance Finally, we analyze the computation overhead of ACMP in generating an optimal motion plan. Table 4 shows the empirical distribution of the computation time for 10000 executions of each method in either simulation. From Table 4, the difference in average computation time between SCMP and ACMP is about 130 ms in the quadrotor case and 7 ms in the UUV case. This result is because SCMP considers the optimization of all relaxable constraints while ACMP only considers the optimization of relaxable constraints that are predicted to be unsatisfiable. So SCMP requires more time of computation, especially when there are more relaxable constraints to be considered.

Table 4: Statistics on Computation Duration.

Cases	*Approaches*	*Average* [s]
Quadrotor	SCMP	0.2115
	ACMP	***0.0811***
UUV	SCMP	0.0423
	ACMP	***0.0344***

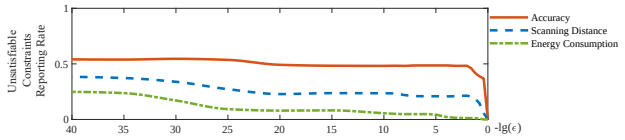

Figure 6: Unsatisfiable constraints reporting rate. (UUV case, # of disturbances = 9)

Choice of violation tolerance As discussed in the paper, the choice of violation tolerances ε determines which constraint needs relaxation, while the larger the value is, the less number of constraints in the ε-unsatisfiable constraints set ($\mathcal{C}_{na}$), along with the underlying higher risk of no feasible solution in the step of *Constraints Satisfaction Optimization*. Thus the value of ε should be delicately determined based on experimental data. As illustrated in Fig. 5(a), the increase of violation tolerance may lead to the decreases in constraint satisfaction as no violation would be reported when the violation degree is smaller than the tolerance. Fig. 6 illustrates the possibilities that relaxable constraints are reported as unsatisfiable in the UUV case, as the increase of violation tolerance increases. In the UUV case, we choose $\varepsilon_{l,E,\varphi} = \{0, 0, 10^{-3}\}$, when the possibility of reporting unsatisfiable constraints tends to be gentle.

References

Burian, S. J.; Velugubantla, S. P.; Chittineni, K.; Maddula, S. R. K.; and Brown, M. J. 2002. Morphological analyses using 3D building databases: Portland, Oregon. Technical report, Utah. LA-UR, Los Alamos National Laboratory, Los Alamos, NM.

Hidalgo-Panagua, A.; Vega-Rodríguez, M. A.; Ferruz, J.; and Pavón, N. 2017. Solving the multi-objective path planning problem in mobile robotics with a firefly-based approach. *Soft Computing* 21(4): 949–964.

Luo, Y.; Yu, Y.; Jin, Z.; Li, Y.; Ding, Z.; Zhou, Y.; and Liu, Y. 2020. Privacy-Aware UAV Flights through Self-Configuring Motion Planning. In *Proc. ICRA 2020*, 1169–1175.

Shevtsov, S.; and Weyns, D. 2016. Keep it SIMPLEX: satisfying multiple goals with guarantees in control-based self-adaptive systems. In *Proc. SIGSOFT FSE 2016*, 229–241.

Shevtsov, S.; Weyns, D.; and Maggio, M. 2019. SimCA*: A control-theoretic approach to handle uncertainty in self-adaptive systems with guarantees. *ACM Transactions on Autonomous and Adaptive Systems (TAAS)* 13(4): 17.

Xiong, R.; and Shan, F. 2018. DroneTank: Planning UAVs' Flights and Sensors' Data Transmission under Energy Constraints. *Sensors* 18(9): 2913:1–2913:19.